Inorganic Chemistry

Article

pubs.acs.org/IC

Solid-State and Solution-State Coordination Chemistry of Lanthanide(III) Complexes with α-Hydroxyisobutyric Acid

Xiao-Yan Chen,[†] George S. Goff,*[,†] William C. Ewing,[†] Brian L. Scott,[‡] and Wolfgang Runde*[,§]

[†]Chemistry Division, [‡]Material Physics and Applications Division, and [§]Science Program Office, Los Alamos National Laboratory, Los Alamos, New Mexico 87545, United States

Supporting Information

ABSTRACT: Despite the wide range of applications of α-hydroxyisobutyric acid (HIBA) in biochemical processes, pharmaceutical formulations, and group and elemental separations of lanthanides and actinides, the structures and geometries of lanthanide−HIBA complexes are still not well understood. We reacted HIBA with lanthanides in aqueous solution at pH = 5 and synthesized 14 lanthanide−HIBA complexes of the formula $[Ln(HIBA)_2(H_2O)_2](NO_3)\cdot H_2O$ (Ln = La (**1**), Ce (**2**), Pr (**3**), Nd (**4**), Sm (**5**), Eu (**6**), Gd (**7**), Tb (**8**), Dy (**9**), Ho (**10**), Er (**11**), Tm (**12**), Yb (**13**), Lu (**14**)), isolating single crystals (**1**−**7**, **10**, and **11**) and powders (**8**, **9**, and **12**−**14**). Both single-crystal and powder X-ray diffraction studies reveal a two-dimensional extended structure across the entire lanthanide series. The environment around the eight-coordinated Ln(III) atom is best described as a distorted dodecahedron, where HIBA acts as a monoanionic tridentate ligand with one carboxylato oxygen atom and one hydroxyl oxygen atom chelating to one Ln(III) center. The carboxylato oxygen atom from a second HIBA ligand bridges to a neighboring Ln(III) atom to form a two-dimensional extended structure. While the coordination mode for HIBA is identical across the lanthanide series, three different structure types are found for La, Ce−Ho, and Er−Lu. Solution characterization using ^{13}C NMR further confirmed a single solution complex under the crystallization conditions. Raman and UV−vis−NIR absorbance and diffuse reflectance spectra of HIBA−Ln(III) complexes were also measured.

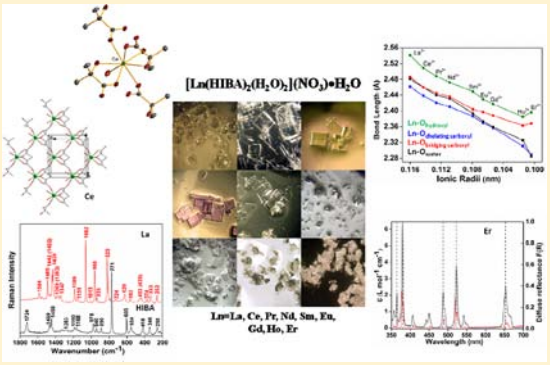

INTRODUCTION

Hydroxycarboxylic acids are an important class of chemicals with a wide range of applications including biodegradable plastics, cleaning agents, food additives, and pharmaceutical formulations.[1] α-Hydroxyisobutyric acid (HIBA, $C_4H_8O_3$, CAS no. 565-70-8) is a characteristic human metabolite that can be used as a biomarker for diagnosing and tracking metabolic disorders such as lactic acidosis[2] and diabetes.[3] In pharmaceutical formulations HIBA is being used as both a pharmacologically inactive carrier and part of the active ingredients.[4] HIBA can be found in the geosphere as a degradation product of humic substances[5] and also as a byproduct from paper manufacturing.[6] Because of its biological importance and similarity to other biologically active compounds (such as sugars and amino acids) understanding the coordination chemistry of HIBA with metal ions is of great interest.

Due to their unique magnetic, optical, and catalytic properties, research into utilizing rare earth compounds in industrial, technological, and medical applications has been continuously growing over the last few decades. Additionally, the lanthanides constitute about one-fourth of the total fission products produced in nuclear fission of uranium or plutonium.[7] HIBA was first used in 1956 as a superior reagent to separate individual members of the lanthanide series from a complex mixture using a Dowex 50 cation-exchange resin[8,9] and in 1997 was identified as an efficient separation reagent for the discovery of the transplutonium elements.[10] Although many chelating agents have been tested and used for lanthanide chromatographic separations, HIBA remains the premier separating reagent.

The dual hydroxyl and carboxyl functionality enables various coordination modes for HIBA (Scheme 1), in which the hydroxyl group could either be protonated or be deprotonated. Although HIBA has been utilized as an eluent to separate lanthanides and actinides for many years,[8−17] the eluted products in solution were generally not structurally characterized and information on the coordination of lanthanides with HIBA remains rare. Several researchers have reported that HIBA most likely forms negatively charged solution complexes with the lanthanides of the general formula $Ln(HIBA)_4^-$.[18−20] The trivalent lanthanides are assumed to adopt either a six-coordinate geometry with two HIBA acting as bidentate ligands (Scheme 1c or 1d) and the other two as monodentate (Scheme 1a or 1b) or an eight-coordinate geometry with four HIBA as bidentate chelating ligands.

Only a few crystal structures have been reported in the literature for HIBA−metal ion complexes. Carballo et al.

Received: August 14, 2012
Published: December 5, 2012

   dx.doi.org/10.1021/ic301775d | Inorg. Chem. 2012, 51, 13254−13263

Scheme 1. Possible Coordination Modes of HIBA with Metal Ions

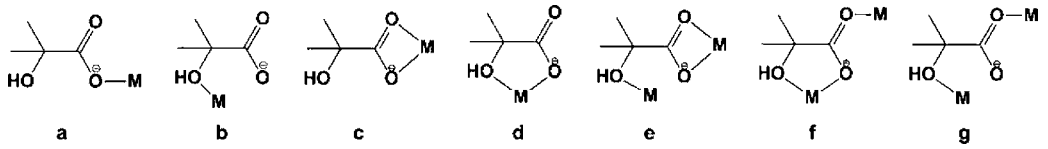

reported the structures of HIBA complexes with dioxovanadate(V),[21] germanium(IV),[22] copper(II),[23] cobalt(II),[24] manganese(II),[25] and zinc(II).[25,26] In all of these complexes, HIBA acts as a monoanionic (O,O′)-bidentate ligand that chelates the metal cations through both carboxyl and hydroxyl groups (Scheme 1e). Despite the fact that HIBA has been used in lanthanide separations for over 55 years, there is only one reported crystal structure of a lanthanide with HIBA, $La(HIBA)_2{\cdot}Cl{\cdot}2H_2O$.[27] The authors describe the structure as a one-dimensional polymeric chain, in which eight-coordinate La(III) atoms are connected via bridging carboxyl groups (Scheme 1f). On the basis of powder X-ray diffraction data the authors hypothesize the existence of two different structure types across the lanthanide series with the structural break at Pr(III). Unfortunately, the authors did not provide any details of the powder X-ray diffraction analysis and failed to elaborate on the nature of the proposed second lanthanide−HIBA complex.

Over the past few years our research group has focused on developing a fundamental understanding of lanthanide and actinide solubility and speciation in nonconventional environments, such as concentrated carbonate solutions, to exploit their differences for used nuclear fuel reprocessing.[28−38] Since HIBA can form complexes with both lanthanides and actinides, it is critical to understand the coordination chemistry of HIBA with the f elements. In order to fill this knowledge gap, we reacted the lanthanides with HIBA in aqueous solutions at pH = 5 and synthesized 14 solid complexes of general formula $[Ln(HIBA)_2(H_2O)_2](NO_3){\cdot}H_2O$. The isolated solid compounds have been characterized by Raman spectroscopy and single-crystal/powder X-ray diffraction. In order to explore the coordination chemistry in solution we used UV−vis−NIR spectroscopy and ^{13}C NMR spectroscopy.

EXPERIMENTAL METHODS

All chemicals were purchased from Fisher Scientific, Inc., and solutions were prepared from distilled deionized water with a specific resistance ≥ 18.0 MΩ·cm. Lanthanide stock solutions were prepared gravimetrically by dissolving $Ln(NO_3)_3{\cdot}6H_2O$ (99.99% purity) in purified water.

Fourteen lanthanide(III) complexes (La (**1**), Ce (**2**), Pr (**3**), Nd (**4**), Sm (**5**), Eu (**6**), Gd (**7**), Tb (**8**), Dy (**9**), Ho (**10**), Er (**11**), Tm (**12**), Yb (**13**), Lu (**14**)) with HIBA in aqueous solutions were prepared by adding 0.5 mL of 1 M Ln(III) nitrate stock to 5 mL of 0.2 M HIBA solution. The pH was adjusted to 5 by adding 1 M NaOH and remained constant throughout the crystallization experiments. The pH of the HIBA solution was chosen to mimic the conditions of column chromatographic lanthanide separation as reported in the literature (pH varies between 3 and 5, the pK_a of HIBA is 3.79).[8−17] The resulting solution was filtered through a 0.45 μm polyamide syringe filter and transferred to a 20 mL borosilicate scintillation vial, allowing for slow evaporation at room temperature until precipitation occurred. The ligand to metal ratio was varied from 1:1 to 4:1, with the most favorable crystallization conditions at 2:1. Crystals of **1**−**7**, **10**, and **11** formed within 4−5 days, and their structures were determined by single-crystal X-ray diffraction. Experiments for **8**−**9** and **12**−**14** formed amorphous precipitates over the course of a week, which were studied by powder X-ray diffraction. Crystals of **1**−**7**, **10**, and **11** were isolated, and their structures were determined by single-crystal X-ray diffraction studies.

Additional characterization was performed using conventional UV−vis−NIR diffuse reflectance and Raman spectroscopy. Raman spectra of solid samples were collected for all compounds with a Thermo Scientific DXR SmartRaman spectrometer with a 780 nm excitation laser. Diffuse reflectance spectra were measured for ground samples of **3**−**6** and **9**−**11** using a Cary 5 UV−vis−NIR spectrophotometer with a diffuse reflectance attachment, and solution spectra were obtained using a Cary 5 UV−vis−NIR spectrophotometer. Compounds **1** and **14** dissolved in water were also characterized by ^{13}C NMR spectroscopy. Measurements were obtained at room temperature using a Bruker ARX-300 spectrometer equipped with 5 and 10 mm multinuclear probes. The frequency was 75 MHz for the ^{13}C nuclei.

Crystals were removed from solution, mounted using a nylon cryoloop and Paratone-N oil, and cooled to 120 K using a liquid nitrogen vapor stream. Data were collected on a Bruker D8 diffractometer, with an APEX II charge-coupled-device (CCD) detector, and a Bruker Kryoflex low-temperature device. The instrument was equipped with a graphite-monochromatized Mo Kα X-ray source (λ = 0.71073 Å). A hemisphere of data was collected using ω scans, with 10 s frame exposures and 0.5° frame widths. Data collection and initial indexing and cell refinement were handled using APEX II software.[39] Frame integration, including Lorentz-polarization corrections, and final cell parameter calculations were carried out using SAINT+ software.[40] Data were corrected for absorption using redundant reflections and the SADABS program.[41] Decay of reflection intensity was not observed as monitored via analysis of redundant frames. The structure was solved using direct methods and difference Fourier techniques. Hydrogen atom positions were idealized on methyl and hydoxyl groups but were not refined on water molecules. Final refinement included anisotropic temperature factors on all nonhydrogen atoms. Structure solution, refinement, and creation of publication materials were performed using SHELXTL.[42] Powder X-ray diffraction data were collected on a Bruker D8 Advance diffractometer. The instrument was configured with Ni-filtered Cu Kα (1.54059 Å) radiation and a silicon strip detector (Lynxeye).

RESULTS AND DISCUSSION

Crystal Structures. Reaction of lanthanides with HIBA resulted in formation of single crystals for 9 out of the 14 lanthanides. Figure 1 shows photographs of the clear rectangular plates formed. Crystallographic analysis revealed the crystals to be $Ln(HIBA)_2(H_2O)_2](NO_3){\cdot}H_2O$ with Ln = La (**1**), Ce (**2**), Pr (**3**), Nd (**4**), Sm (**5**), Eu (**6**), Gd (**7**), Ho (**10**), and Er (**11**). Tables 1 and 2 show the important crystallographic parameters for complexes **1**−**7**, **10**, and **11**. Complete crystallographic details can be found in the Supporting Information (Table S1).

Single-crystal X-ray analysis reveals that there are three distinct crystallographic structures across the lanthanide series. Figure 2 illustrates the three-dimensional packing of the three different structure types, which are compared below.

*a. $La(HIBA)_2(H_2O)_2](NO_3){\cdot}H_2O$ (**1**).* This is the only compound that crystallizes in the triclinic space group *P*-1. The unit cell contains two unique La(III) atoms, one unique nitrate (N1), and one unique lattice water (O24) which is split between the two unique lanthanum centers (one-half each, Figure 3). A second nitrate anion (N2) is disordered across an

dx.doi.org/10.1021/ic301775d | Inorg. Chem. 2012, 51, 13254−13263

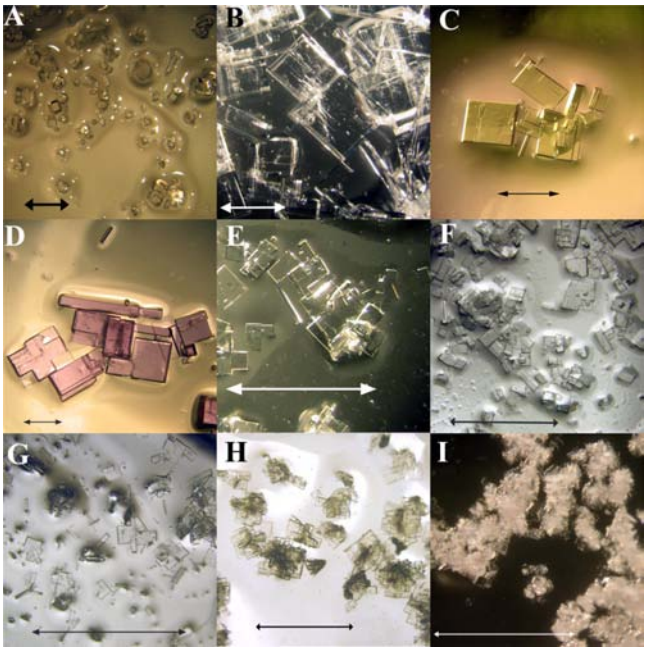

Figure 1. Photographs of single crystals $[Ln(HIBA)_2(H_2O)_2](NO_3)\cdot H_2O$, Ln = La (A), Ce (B), Pr (C), Nd (D), Sm (E), Eu (F), Gd (G), Ho (H), and Er (I). Scale shows a 1 mm arrow for A–G and a 0.5 mm arrow for H and I.

inversion center and shares partial occupancy with a second water molecule (O22 or O23). The extended Ln–HIBA layers lie in the crystallographic *bc* plane, separated by layers of nitrate anions and lattice waters. The oxygen-containing functional groups in the HIBA ligand and the presence of nitrate counteranions and lattice waters enables formation of an extended architecture based on a hydrogen-bonding network.

*b. $[Ln(HIBA)_2(H_2O)_2](NO_3)\cdot H_2O$ (Ln = Ce (**2**), Pr (**3**), Nd (**4**), Sm (**5**), Eu (**6**), Gd (**7**), and Ho (**10**)).* Complexes **2**–**7** and **10** are isostructural, crystallizing in the monoclinic space group *C*2/*c*. A 2-fold rotation axis bisects the H_2O–Ln–OH_2 angle, and the Ln(III) centers occupy sites of crystallographic symmetry. In contrast to **1**, this structure type has only one unique Ln(III) center in the unit cell, one disordered nitrate anion, and one disordered lattice water. The nitrate anion (N1) is also disordered across an inversion center, and one oxygen atom of the nitrate is half-occupied with the lattice water (O5). This is the same disorder observed in **1** for the second nitrate anion (N2 and O22 or O23). The three-dimensional packing of these monoclinic complexes is different from that of complex **1** due to differences in the water–nitrate sublattice (Figure 2). Figure 3 shows the 50% occupancy split between the disordered nitrate anion and a disordered water molecule.

*c. $[Er(HIBA)_2(H_2O)_2](NO_3)\cdot H_2O$ (**11**).* Multiple efforts in isolating high-quality crystals of compound **11** failed, and only twinned crystals could be isolated. The stoichiometry and HIBA coordination mode in **11** are the same as those of complexes **2**–**7** and **10**. However, the 2-fold rotation axis bisecting the H_2O–Ln–OH_2 angle found in complexes **2**–**7** and **10** is absent for the Er(III) complex. Instead, the two twinned structures are related by a 2-fold symmetry. The disorder of water molecules near the nitrate is also different from the previous structures. While the nitrate anions are still disordered across an inversion center, the water molecule (O12) occupies a distinct crystallographic site within the unit cell (Figure 3).

The three-dimensional packing diagrams for $[La(HIBA)_2(H_2O)_2](NO_3)\cdot H_2O$ (**1**), $[Ce(HIBA)_2(H_2O)_2]$-

Table 1. Selected Crystal Data and Structure Refinements for $[Ln(HIBA)_2(H_2O)_2](NO_3)\cdot H_2O$ (1–5)

	1	2	3	4	5
formula	$C_8H_{20}LaNO_{12}$	$C_8H_{20}CeNO_{12}$	C_8H_{20} $PrNO_{12}$	$C_8H_{20}NdNO_{12}$	$C_8H_{20}SmNO_{12}$
fw	461.16	462.37	463.16	466.49	472.60
cryst syst	triclinic	monoclinic	monoclinic	monoclinic	monoclinic
space group	*P*-1	*C*2/*c*	*C*2/*c*	*C*2/*c*	*C*2/*c*
a (Å)	6.2849(4)	9.0101(7)	8.9898(7)	8.9585(11)	8.903(3)
b (Å)	12.5728(7)	8.6571(7)	8.6316(7)	8.6012(10)	8.533(3)
c (Å)	21.7514(13)	21.0265(17)	20.9864(16)	21.014(3)	20.973(8)
α (deg)	104.3980(10)	90.00	90.00	90.00	90.00
β (deg)	91.6040(10)	93.1900(10)	93.1100(10)	92.9167(13)	92.771(4)
γ (deg)	92.3850(10)	90.00	90.00	90.00	90.00
V (Å^3)	1662.04(17)	1637.6(2)	1626.1(2)	1617.1(3)	1591.4(10)
Z	4	4	4	4	4
ρ (g/cm^3)	1.843	1.875	1.892	1.916	1.972
μ (mm^{-1})	2.627	2.837	3.054	3.269	3.749
F(000)	912	916	920	924	932
cryst size (mm)	0.22 × 0.12 × 0.04	0.20 × 0.08 × 0.06	0.16 × 0.10 × 0.04	0.14 × 0.06 × 0.04	0.18 × 0.14 × 0.04
θ (deg)	1.93–28.37	1.94–28.29	1.94–28.45	1.94–28.35	1.94–28.27
index ranges	$-8 \le h \le 8$	$-11 \le h \le 11$	$-11 \le h \le 11$	$-11 \le h \le 11$	$-11 \le h \le 11$
	$-16 \le k \le 16$	$-11 \le k \le 11$	$-11 \le k \le 11$	$-11 \le k \le 11$	$0 \le k \le 11$
	$-28 \le l \le 28$	$-27 \le l \le 27$	$-27 \le l \le 27$	$-27 \le l \le 27$	$-26 \le l \le 0$
min and max transmission	0.5957 and 0.9022	0.6008 and 0.8482	0.6408 and 0.8876	0.6576 and 0.8804	0.5518 and 0.8645
GOF on F^2	1.556	1.446	1.269	1.099	1.929
R_1, R_2 [$I > 2\sigma(I)$]	0.0232, 0.0718	0.0212, 0.0614	0.0197, 0.0567	0.0304, 0.0826	0.0322, 0.0773
R_1, R_2 (all data)	0.0295, 0.0796	0.0213, 0.0615	0.0202, 0.0569	0.0313, 0.0831	0.0325, 0.0774
largest diff peak and hole (e·Å^{-3})	1.050 and −0.603	1.061 and −0.889	0.947 and −0.864	0.690 and −1.248	0.972 and −1.498

dx.doi.org/10.1021/ic301775d | *Inorg. Chem.* 2012, 51, 13254–13263

Table 2. Selected Crystal Data and Structure Refinements for $[Ln(HIBA)_2(H_2O)_2](NO_3)\cdot H_2O$ (6, 7, 10, and 11)

	6	7	10	11
formula	$C_8H_{20}EuNO_{12}$	$C_8H_{20}GdNO_{12}$	$C_8H_{20}HoNO_{12}$	$C_8H_{20}ErNO_{12}$
fw	474.21	479.50	487.18	489.51
cryst syst	monoclinic	monoclinic	monoclinic	monoclinic
space group	$C2/c$	$C2/c$	$C2/c$	$C2/c$
a (Å)	8.8830(7)	8.8635(10)	8.8084(16)	8.3811(14)
b (Å)	8.5107(7)	8.4868(9)	8.4031(15)	8.7062(14)
c (Å)	20.9290(16)	20.917(2)	20.874(4)	21.369(4)
β (deg)	92.5960(10)	92.5150(10)	92.136(2)	96.6087(18)
V (Å^3)	1580.6(2)	1571.9(3)	1544.0(5)	1548.9(4)
Z	4	4	4	4
ρ (g/cm^3)	1.993	2.026	2.096	2.099
μ (mm^{-1})	4.027	4.279	5.185	5.479
$F(000)$	936	940	952	956
cryst size (mm)	0.14 × 0.08 × 0.02	0.14 × 0.08 × 0.02	0.12 × 0.06 × 0.02	0.18 × 0.08 × 0.02
θ (deg)	1.95−28.46	1.95−28.26	1.95−28.25	1.92−28.45
index ranges	$-11 \le h \le 11$	$-11 \le h \le 11$	$-11 \le h \le 11$	$-11 \le h \le 11$
	$-11 \le k \le 11$	$-11 \le k \le 11$	$-11 \le k \le 10$	$0 \le k \le 11$
	$-26 \le l \le 27$	$-26 \le l \le 26$	$-27 \le l \le 27$	$0 \le l \le 27$
min and max transmission	0.6025 and 0.9238	0.5857 and 0.9193	0.5750 and 0.9034	0.4388 and 0.8983
GOF on F^2	1.167	1.204	2.566	1.303
R_1, R_2 $[I > 2\sigma(I)]$	0.0158, 0.0449	0.0201, 0.0506	0.0525, 0.1336	0.0415, 0.1420
R_1, R_2 (all data)	0.0164, 0.0456	0.0223, 0.0513	0.0548, 0.1339	0.0424, 0.1426
largest diff peak and hole (e·Å^{-3})	0.860 and −0.508	0.759 and −0.923	3.003 and −5.470	1.807 and −2.867

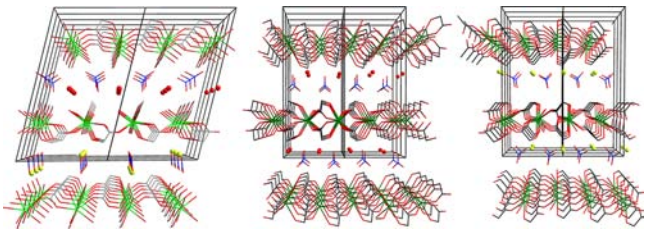

Figure 2. Three-dimensional packing of $[Ln(HIBA)_2(H_2O)_2](NO_3)\cdot H_2O$ (Ln = La, left; Ce, middle; Er, right) viewed along the a axis: Ln, green; C, gray; O, red; disordered water molecule, red balls; ordered lattice water molecules, light green balls. Hydrogen atoms and methyl groups on HIBA are omitted for clarity.

$(NO_3)\cdot H_2O$ (**2**), and $[Er(HIBA)_2(H_2O)_2](NO_3)\cdot H_2O$ (**11**) shown in Figure 2 illustrate complex networks of hydrogen bonding. Complex **2** is chosen to discuss the crystallographic features found in complexes **2**−**7** and **10**. In **1** there are four types of hydrogen bonding: (1) between the hydroxyl oxygen atom of coordinated HIBA and the oxygen atom of disordered nitrate (O···O, 2.739 and 2.762 Å), (2) between the hydroxyl oxygen atom of coordinated HIBA and the oxygen atom of disordered lattice water (O···O, 2.733 and 2.742 Å), (3) between the oxygen atom of coordinated water and the oxygen atom of the disordered nitrate (O···O, 2.722 Å), and (4) between the oxygen atom of coordinated water and the oxygen atom of lattice water (O···O, 2.660 Å). The O···O distances are in the usual range for complexes with HIBA ligands.[21−27] The two-dimensional sheets of the cationic units in **1** are linked together by hydrogen bonds to form a three-dimensional network with the nitrate anions arranged alternatively between the two-dimensional sheets. In Figure 2, the disordered nitrate anion lies between the first two layers and is only shown at one occupancy position, while the other 50% occupancy position is represented by a disordered water molecule (red balls). The

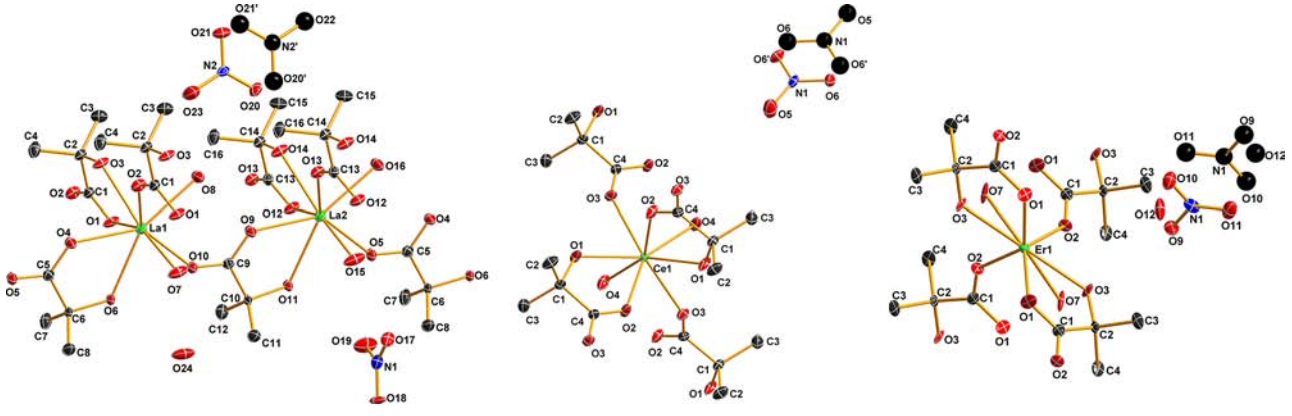

Figure 3. Thermal ellipsoids (50% probability) of $[Ln(HIBA)_2(H_2O)_2](NO_3)\cdot H_2O$, where Ln = La (left), Ce (middle), and Er (right). Hydrogen atoms have been removed for clarity. Disordered nitrate is shown in black balls.

dx.doi.org/10.1021/ic301775d | Inorg. Chem. 2012, 51, 13254−13263

ordered lattice water molecules are shown in light green (Figure 2).

Compared to complex **1**, the hydrogen bonds between HIBA and disordered water and coordinated water and lattice water are missing in the complex **2** structure type. The O···O bond distances in **2** are comparable to those found in **1**: (1) hydroxyl oxygen atom of coordinated HIBA ligand and oxygen atom of disordered nitrate anion (O···O, 2.756 and 2.775 Å); (2) coordinated water oxygen atom and oxygen atom of disordered nitrate anion (O···O, 2.731 Å). A third hydrogen-bonding mode between oxygen atoms of two neighboring nitrate anions (O···O, 2.919 Å) is not observed in **1**. The hydrogen bonding between the disordered nitrate anions and two-dimensional cation sheets lead to a three-dimensional network with disordered nitrate anions sandwiched between the cationic sheets.

In complex **11**, only two types of hydrogen bonding are observed to link the 2D sheets in the *c* direction: (1) oxygen atom of the HIBA hydroxyl group and oxygen atom of disordered nitrate (O3···O11, 2.784 Å) and (2) coordinated water oxygen atom and oxygen atom of nitrate anion (O7···O10, 2.719 Å).

All isolated lanthanide compounds exhibit the same coordination geometry around the lanthanide atom, as shown in Figure 3. The Ln(III) atoms are eight coordinate with four oxygen atoms from two chelating HIBA ligands, two oxygen atoms from two bridging HIBA ligands, and two coordinated water molecules completing the distorted dodecahedron coordination geometry. In all of the structures, HIBA adopts a monoanionic tridentate coordination (Scheme 1f) with the lanthanide atom. Oxygen atoms from both the hydroxyl and the carboxylate groups chelate the Ln atom while the second carboxylate oxygen atom bridges to neighboring Ln atoms. This is in stark contrast to previously reported crystal structures of HIBA–transition metal complexes,[21−26] in which the HIBA acts as a bidentate monoanion coordinating the metal atoms with two oxygen atoms from the carboxylate and hydroxyl groups (Scheme 1d). In the present Ln–HIBA complexes, each Ln(III) atom forms two 5-membered rings by coordinating two HIBA ligands via their hydroxyl oxygen and carboxylate oxygen atoms. The coordination of the Ln(III) atom causes electron delocalization in the carboxylate groups. For example, the two C–O bond lengths are 1.197(3) and 1.307(3) Å in the free HIBA ligand are quite different,[43] while these bond lengths are very similar in **1** (1.239(3) and 1.280(3) Å).

The chelating and bridging coordination of HIBA creates a two-dimensional sheet structure in the *ab* plane as shown in Figure 4. Neighboring Ln(III) atoms within the layer are linked by bridging carboxyl groups to form a parallelogram lattice with dimensions defined in Figure 5. As the ionic radius of the Ln(III) atoms decreases across the lanthanide series the dimensions of the parallelogram, *x*, *y*, and *z*, are shrinking (Figure 5), while the θ angle steadily increases from Ce to Ho, with La(III) and Er(III) lying above and below the Ln(III) trend line, respectively. The deviations in the La and Er complexes arise from subtle differences in the 2D lattice. In the triclinic structure of **1**, the 2D lattice is oriented with the HIBA ligands bridging between adjacent La centers which are oriented parallel to the *a* and *b* axes (Figure 4 left). The base unit of the parallelogram for the 2D lattice of **1** can best be described as a rhomboid, where x_1 and x_2 have different values of 6.2849 and 6.2859 Å. This is in good agreement with the La–La distance of 6.261 Å previously reported in La-

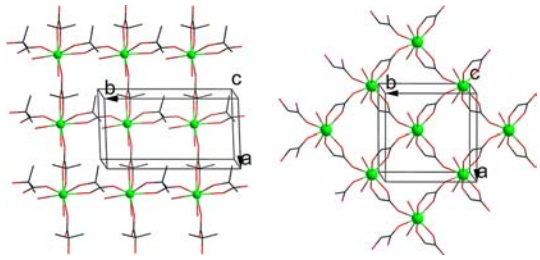

Figure 4. Illustration of the two-dimensional sheet of [La-$(HIBA)_2(H_2O)_2$]$(NO_3)\cdot H_2O$ (**1**, left) and [Ce$(HIBA)_2(H_2O)_2$]-$(NO_3)\cdot H_2O$ (**2**, right). Hydrogen atoms, nitrate anions, and lattice water molecules are omitted for clarity. Color code: O, red; Ln, green; C, gray.

$(HIBA)_2\cdot Cl\cdot 2H_2O$.[27] The relationship between the unit cell dimensions and the rhomboid unit of **1** is defined as $a = x_1$ and $b = 2x_2$. The remaining complexes, including **11** (Er), are monoclinic, and the lattice has been rotated approximately 45° so that the HIBA ligands are no longer oriented along the axes (Figure 4 right). In this case, the lanthanides opposite each other in the parallelogram are oriented along the *a* and *b* axes. The basic unit of the parallelogram for the 2D lattice of **2**–**7**, **10**, and **11** can best be described as a rhombus, where $x_1 = x_2$. For the complexes of Ce through Ho, the relationship between the unit cell dimensions and the rhombic unit is defined as $a = z$ and $b = y$. The unit cell for Er (**11**) is rotated 180° so that $a = y$ and $b = z$.

Figure 6 illustrates the changes in the coordination geometry of the two *cis*-HIBA ligands bridging between adjacent lanthanide centers for the Ho and the Er compounds. For the Ce, Pr, Nd, Sm, Eu, Gd, and Ho complexes, the water–Ln–water (O4–Ln–O4) bond angle varies from 96.83(10)° for Ce to 95.7(3)° for Ho, which is smaller than the bridging carboxylate–Ln–carboxylate bond angle for Ho (O3–Ln–O3, 138.7(3)°). The chelating hydroxyl–Ln–hydroxyl (O1–Ln–O1) bond angle increases from 119.91(8)° (Ce) to 122.8(3)° (Ho). For the Er complex, **11**, the water–Ln–water (O7–Er–O7) bond angle widens to 129.7(6)° and is now larger than the bridging carboxylate–Ln–carboxylate bond angle (O2–Er–O2), which shrinks to 80.4(6)°. The chelating hydroxyl–Ln–hydroxyl (O3–Er–O3) bond angle has also changed dramatically and is almost linear at 178.8(5)° lying along the *c* axis. In Figure 6, the wide angle for the bridging carboxylate–Ln–carboxylate bond angle (O1–Ho–O1) is oriented *up* along the *b* axis. In the Er structure, the wide angle for the bridging carboxylate–Ln–carboxylate bond angle (O2–Er–O2) is oriented *down* along the *b* axis and the *a* and *b* axes have effectively been switched in this structure.

With the exception of the Er(III) complex, the Ln–O bond lengths decrease across the lanthanide series following the well-known lanthanide contraction (Figure 7). In all complexes, the $Ln-O_{hydroxyl}$ bonds are longer than the Ln–O bonds with coordinated water or carboxylate groups. The average bond length of the chelating carboxylato oxygen atom with Ln(III) is slightly shorter than that of the bridging carboxylato oxygen atom with Ln(III); however, while the $Ln-O_{chelating\ carboxylato}$ bond length steadily decreases along the lanthanide series, the bond length for the bridging $Ln-O_{carboxylato}$ seems to undergo less contraction with the heavy lanthanides beyond Sm. This trend is also reflected in the behavior of the $Ln-O_{water}$ bond. For the light lanthanides La–Nd, the $Ln-O_{water}$ bond length tracks the trend of the longer bridging $Ln-O_{carboxylato}$ bond.

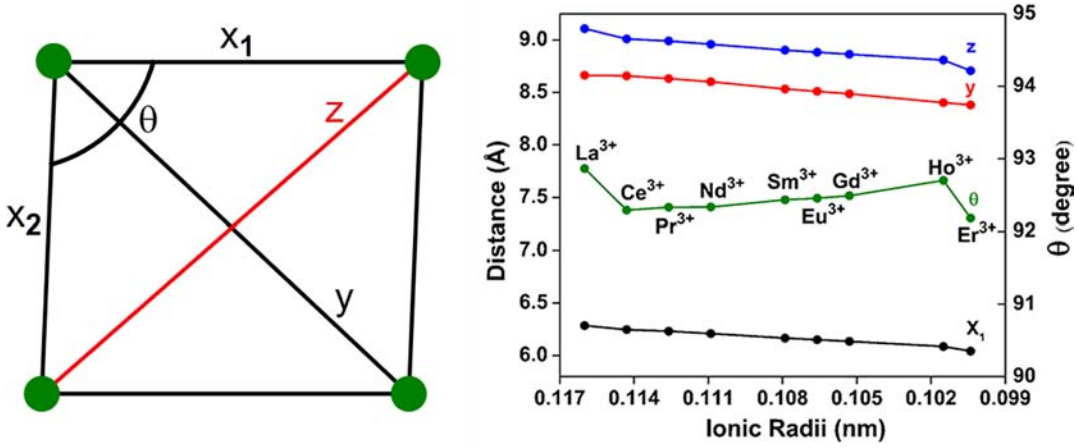

Figure 5. (Left) Scheme of the rhomboidal unit of the two-dimensional sheet of $[Ln(HIBA)_2(H_2O)_2](NO_3)\cdot H_2O$: Ln, green balls. (Right) Size of the rhombic unit with decreasing ionic radii: x_1, black; y, red; z, blue; θ, green. Ionic radii for the eight-coordinate lanthanide cations was taken from Shannon et al.[44]

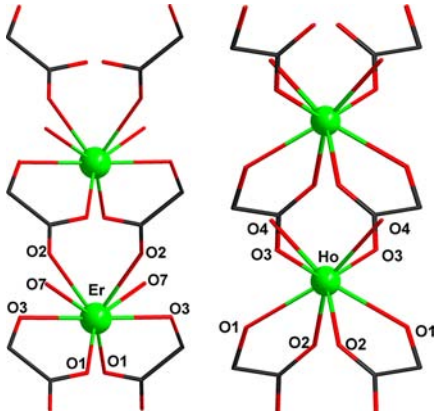

Figure 6. Comparison of the bond angles in $[Ho(HIBA)_2(H_2O)_2]\cdot(NO_3)\cdot H_2O$ (left) and $[Er(HIBA)_2(H_2O)_2](NO_3)\cdot H_2O$ (right) viewed along the a axis: C, gray; O, red.

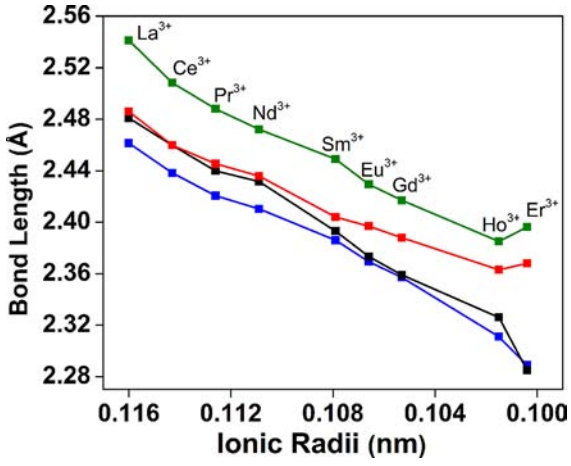

Figure 7. Comparison of the average Ln–O bond lengths with decreasing ionic radii across the lanthanide series:[44] $Ln-O_{hydroxyl}$, green; $Ln-O_{chelating\ carboxylato}$, blue; $Ln-O_{bridging\ carboxylato}$, red; $Ln-O_{water}$, black. Ionic radii for the eight-coordinate lanthanide cations was taken from Shannon et al.[44]

With the deviation of the bridging $Ln-O_{carboxylato}$ bond length from the nearly linear bond length reduction along the lanthanide series and the relative elongation of the $Ln-O_{bridging\ carboxylato}$ bond, the $Ln-O_{water}$ bond shortens tracking the bond length for the heavy lanthanides Sm–Er. The $Er-O_{hydroxyl}$ and $Er-O_{chelating\ carboxylato}$ bond lengths are significantly longer than those of $Ho-O_{hydroxyl}$ and $Ho-O_{chelating\ carboxylato}$, which may be ascribed to the larger cell volume of Er(III) complex (1548.9(4) Å^3) than that of Ho(III) complex (1544.0(5) Å^3) as well as some subtle changes in the Er–HIBA coordination environment which are discussed in the following section.

Powder X-ray Diffraction (PXRD) Analysis. Crystallization experiments for **1**–**7** and **10** produced high-quality single crystals for which the crystallographic structure was determined. For compound **11** (Er) we obtained in limited yield twinned crystals that were sufficient in quality for structure determination. For complexes **12**–**14** only powder precipitates were formed over the period of this study. In order to evaluate the structures and coordination geometries of these powder precipitates we compared the experimental diffraction patterns with both the measured and the simulated diffraction patterns of the single-crystal compounds. PXRD analysis of complexes **1**–**7** and **10** shows excellent agreement between simulated and measured patterns. (PXRD data for all compounds can be found in the Supporting Information (Figures S1–S3)). The Bragg reflections shift to higher theta angle as the ionic radius decreases across the lanthanide series; however, additional Bragg reflections can be observed in the experimental patterns of the heavy lanthanides Er–Lu which cannot be explained using the simulated pattern of the single-crystal structure determined for **11** alone. The additional Bragg reflections match very well with those reflections representing compounds **1**–**10**; thus, erbium represents a transition point in the lanthanide series with a break in the crystal structure. Under our experimental conditions the bulk precipitate is likely coprecipitating as a mixture of the two structure types, which also explains the extreme difficulty of obtaining good-quality crystals of **11**–**14**. While Er appears to be the transition point under the current set of experimental conditions, varying these conditions could result in Ho and Er crystallizing in both structure types. Experimental PXRD patterns for Tm, Yb, and Lu (shown in Figures S3, Supporting Information, and 8) match the measured PXRD pattern for Er very well, indicating that the heavy lanthanides Er–Lu coprecipitate as a mixture of

dx.doi.org/10.1021/ic301775d | Inorg. Chem. 2012, 51, 13254–13263

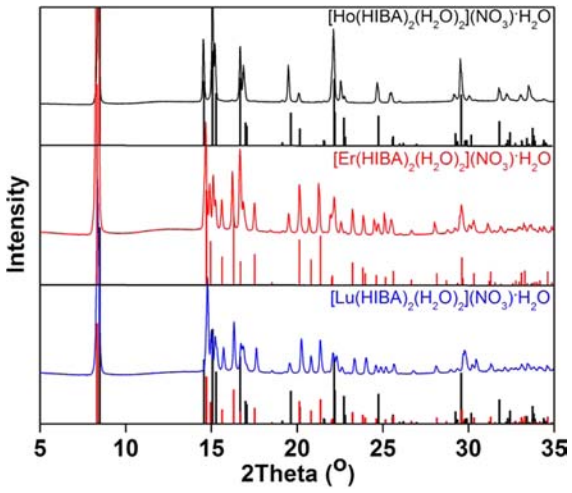

Figure 8. Experimental (lines) and simulated (bars) powder X-ray diffraction patterns of $[Ln(HIBA)_2(H_2O)_2](NO_3)\cdot H_2O$: Ln = Ho (top), Er (center), and Lu (bottom). Simulated Bragg reflections are calculated from the respective $[Ln(HIBA)_2(H_2O)_2](NO_3)\cdot H_2O$ single-crystal structures for Ho and Er.

the structure types identified for both compounds **2**−**10** and **11**. Consequently, the PXRD data is consistent with formation of $[Ln(HIBA)_2(H_2O)_2](NO_3)\cdot H_2O$ across the whole lanthanide series. The ratio of Ln(III):HIBA of 1:2 does not change when varying the metal to ligand ratio in the crystallization experiments from 1:1 to 1:10.

Spectroscopic Characterization. *Solid-State Raman Spectroscopy.* The solid-state Raman spectra for all of the complexes are very similar due to the fact that the coordination modes of HIBA are the same across the lanthanide series (Supporting Information, Figure S5−S6). To date, only Jarmelo et al. reported the Raman frequencies of the free HIBA ligand.[45] The authors attributed the Raman band at 1724 cm^{-1} to the carboxylic symmetric stretching mode ν(C═O) and the Raman band at 1283 cm^{-1} (shoulder) to the carboxylic bending δ(C−O) modes. Figure 9 shows that in the La(III) complex (**1**) the ν(C═O) band at 1584 cm^{-1} is shifted to lower frequency, which is consistent with a longer C═O bond length (1.2514(8) Å) than in the free ligand (1.197(3) Å).[45,46]

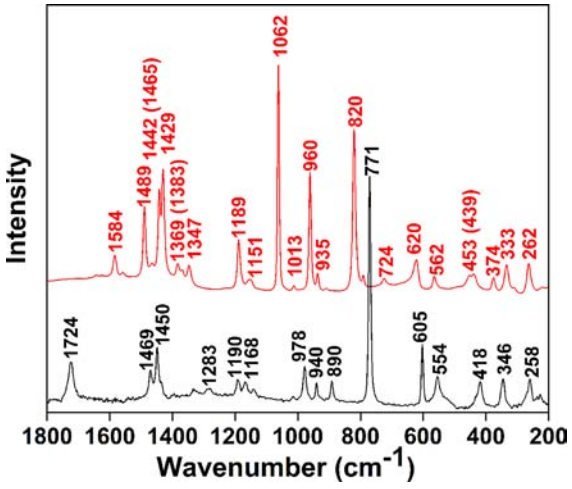

Figure 9. Solid-state Raman spectra of $[La(HIBA)_2(H_2O)_2](NO_3)\cdot H_2O$ (**1**) (red) and HIBA (black).

The higher frequency shifts of the δ(C−O) bands (1283 → 1369 and 1383 cm^{-1}) are also consistent with the shorter C−O bond length: C4−O3, 1.307(3) → 1.2602(2) Å. The Raman band at 1151 cm^{-1} of the hydroxyl ν(C−O) mode shifted to lower frequency by 17 cm^{-1} compared with the hydroxyl ν(C−O) stretching in free HIBA (1168 cm^{-1}). The red shift of the hydroxyl ν(C−O) band can also be explained by coordination of the hydroxyl oxygen atom which results in an elongation of the $C1-O1_{hydroxyl}$ bond from 1.422(3) to 1.4407(3) Å. Analysis of the vibrational spectral shifts for the carboxylic and hydroxyl groups of the La−HIBA complex shows that coordination of the HIBA ligand through the carboxylic (O2) and hydroxyl oxygens (O1) produces red shifts for the carboxylic ν(C═O) and hydroxyl ν(C−O) bands of 140 and 17 cm^{-1}, respectively.

The Raman spectrum of **1** (Figure 9) exhibits the bending modes $\delta(H_2O)$ of coordinated water molecules at 1429 and 1489 cm^{-1}.[47] The ν(C−C) stretching peak is the strongest Raman band for the HIBA ligand at 771 cm^{-1}.[45] This vibrational mode is shifted to 820 cm^{-1} in complex **1**. The bands at 562 and 620 cm^{-1} are due to the bending mode of δ(O═CO) and the torsion mode of τ(C═O), respectively. The bands at 262, 333, and 374 cm^{-1} are assigned to hydroxyl δ(CCO) bending mode, ω(CCC) wagging mode, and γ(CCC), respectively. The new bands observed in the fingerprint region of 400−500 cm^{-1} can be assigned as La−O stretching modes.[48] The increase of the Ln−O stretching frequency from 453 ($La(HIBA)_2(H_2O)_2\cdot NO_3$) to 481 cm^{-1} ($Er(HIBA)_2(H_2O)_2\cdot NO_3$) reflects the increase in Ln−O bond strength due to the lanthanide contraction.

The Raman bands at 3012 and 2981 cm^{-1} are assigned to the asymmetric stretching modes of $\nu(CH_3)$. The symmetric stretching mode of $\nu(CH_3)$ is observed at 2938 cm^{-1} (Figures S4 and S5, Supporting Information). The strong Raman bands at 1442 and 1465 cm^{-1} can be assigned as the asymmetric $\delta(CH_3)$ bending modes, and the weak Raman band at 1347 cm^{-1} is attributed to a symmetric $\delta(CH_3)$ mode. The $\gamma(CH_3)$ modes are observed at 1189 and 960 cm^{-1}. All Raman spectra show broad peaks in the range 3200−3500 cm^{-1} (Supporting Information) which belong to vibrational stretches of the coordinated water molecules. The strongest Raman band observed for **1** is the symmetric stretching mode of the nitrate anion at 1062 cm^{-1}, which is positively shifted from the nitrate stretching bands in $La(NO_3)_3\cdot 6H_2O$ (1048, 1057 cm^{-1}).

UV−vis−NIR Diffuse Reflectance and Solution UV−vis−NIR Spectroscopy. Samples of $[Ln(HIBA)_2(H_2O)_2](NO_3)\cdot H_2O$ (Ln = Pr (**3**), Nd (**4**), Sm (**5**), Eu (**6**), Dy (**9**), Ho (**10**), and Er (**11**)) were characterized by solid state diffuse reflectance spectroscopy and UV−vis−NIR spectroscopy after dissolution in water (Figures S6−S10, Supporting Information). Figure 10 shows the solid state diffuse reflectance spectra for **3** and **11** and of the resulting solution species at pH 5. The electronic absorbances for trivalent lanthanide complexes are characterized by a number of Laporte-forbidden f−f transitions.[49] Solution UV−vis−NIR spectra the molar absorptivities show general agreement with the characteristic f−f transitions for the $Ln^{3+}(aq)$ ion absorbance in diluted acid (Figures S6−S10, Supporting Information).[49−51] Complexation of the Ln(III) ions with HIBA results in only very small shifts of the most prominent absorbances compared to the aquo ion. As an example, the characteristic transitions for Pr(III) at 444 ($^3H_4$ to $^3P_2$), 468 ($^3H_4$ to $^3P_1$), 481 ($^3H_4$ to $^3P_0$), and 589 nm ($^3H_4$ to $^1D_2$)[49,50] are shifted to 442.7, 468.2, 471.3, 482.1, 484.4, 586.1, and 590.7 nm upon complexation with HIBA. Similarly, small

dx.doi.org/10.1021/ic301775d | Inorg. Chem. 2012, 51, 13254−13263

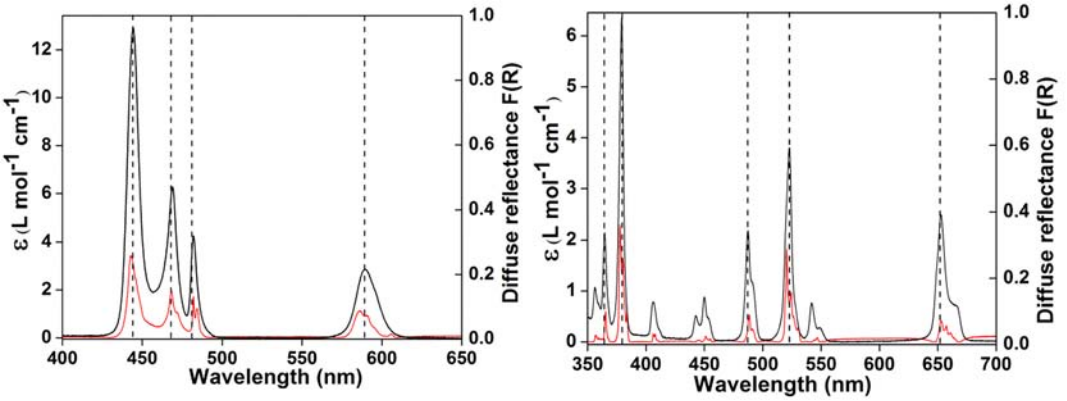

Figure 10. Solution-state UV–vis–NIR spectrum (black) and solid-state UV–vis–NIR diffuse reflectance spectrum (red) of $[Pr(HIBA)_2(H_2O)_2](NO_3)\cdot H_2O$ (**3**, left) and $[Er(HIBA)_2(H_2O)_2](NO_3)\cdot H_2O$ (**11**, right). Ln(III) aquo ion absorbance peaks are shown as dotted lines.[49]

shifts in the primary absorbance peaks relative to the five most intense transitions in the Er(III) aquo ion absorbance spectrum at 364, 379, 487, 523, and 652 nm are observed. The relative intensity ratios and peak positions in the solution state UV–vis–NIR spectra and their solid state UV–vis–NIR diffuse reflectance spectra match well, suggesting similar coordination environments around the lanthanide in solution and the solid state. The solution absorbance and solid state diffuse reflectance patterns of the heavy lanthanides overlap especially well. Larger shifts in the peaks can be observed in the hypersensitive bands for the lighter lanthanides Nd(III) and Sm(III) (Figures S6–S10, Supporting Information).

^{13}C NMR Spectroscopy. To understand the solution speciation during the crystallization experiments we used ^{13}C NMR spectroscopy. Uncomplexed HIBA at pH 5 shows three ^{13}C NMR resonances at 73.07 ppm for the hydroxyl carbon (C1), 26.06 ppm for the methyl carbons (C2/C3), and 183.32 ppm for the carboxyl carbon (C4). ^{13}C NMR spectra of the supernatant of the crystallization experiments for the diamagnetic La(III) and Lu(III) complexes show only one set of signals for the complexed HIBA ligand. All coordinated HIBA ligands in the HIBA–Ln(III) solution complex are equivalent and display the same ^{13}C NMR features shifted from those of the free ligand (Table 3). Similarly, the NMR chemical shifts of the Ln(III) complex redissolved in water at pH 5 are shifted to low frequency compared to the free ligand. When HIBA is chelating a metal ion, the carbon atoms of the COOH and C(OH) groups are deshielded, illustrated as coordination-induced shifts, $\Delta\delta$. The $\Delta\delta$ values of 3.5 (C(OH)) and 0.7 ppm (COOH) for the La(III) solution complex and 4.2 (C(OH)) and 0.4 ppm (COOH) for the Lu(III) solution complex in the supernatant (Table 3) indicate that both the hydroxyl and the carboxyl groups of the HIBA ligand are coordinated with the Ln(III) groups (Scheme 1f). Since the hydroxyl oxygen atoms are protonated, the $\Delta\delta$ values for the carbon atom attached to hydroxyl group (C1) is larger than the $\Delta\delta$ for the deprotonated carboxyl carbon atoms (C4). As expected, the $\Delta\delta$ values for the methyl carbons are smaller than observed for the binding functional groups. Notably, the chemical shifts for the La(III) complex in the supernatant during crystallization are nearly identical to those observed after dissolving the La(III) crystal in water at pH 5, indicating that only one solution complex exists under the conditions investigated.

Table 3. ^{13}C NMR Chemical Shift (δ, ppm) for HIBA at pH = 5, La(III) and Lu(III) Complexes of HIBA

	C1	C2/C3	C4
HIBA (pH = 5)	73.07	26.06	183.32
La(III) complex supernatant	76.59	26.23	184.00
La(III) complex in water (pH = 5)	76.52	26.25	184.05
Lu(III) complex supernatant	77.23	25.68	183.72
Lu(III) complex in water (pH = 5)	77.03	25.76	183.84

CONCLUSION

We synthesized and characterized 14 lanthanide complexes of the form $[Ln(HIBA)_2(H_2O)_2](NO_3)\cdot H_2O$ using single-crystal and powder X-ray diffraction as well as vibrational and absorbance spectroscopies. All complexes reveal a two-dimensional extended structure with bridging HIBA ligands connecting adjacent lanthanide centers in the *ab* plane and a complex network of hydrogen bonding with nitrate ions and lattice waters, which lie between the sheets along the *c* axis. Three different structure types are observed across the lanthanide series with subtle differences in 3D packing and hydrogen networks. Structural breaks are observed at Ce(III) and Er(III). While the coordination geometry around the lanthanide center is the same for all of the lanthanide compounds, the three distinct crystal structures arise. The inner coordination sphere is nearly identical for all complexes, with eight-coordinate Ln(III) centers coordinated with six oxygen atoms from four HIBA ligands and two oxygen atoms from two bound water molecules. HIBA chelates the Ln(III) atoms with one carboxylato oxygen atom and one hydroxyl oxygen atom while bridging neighboring Ln(III) atoms with its other carboxylato oxygen atom. The heaviest lanthanides, Er–Lu, coprecipitate as mixtures of the Ho (**10**) and Er (**11**) structure types, which makes isolation of high-quality crystals extremely difficult.

The coordination geometries for **1**–**7**, **10**, and **11** differ significantly from a previously reported X-ray diffraction study of $Ln(HIBA)_2\cdot Cl\cdot 2H_2O$ compounds in which Lin et al. postulated two distinct lanthanide–HIBA complexes with the structural break occurring between Ce and Pr.[27] Although the inner coordination environment is identical across the lanthanide series, we found three distinct structures with the first structural break occurring between La and Ce and the second occurring between Ho and Er. Lin et al. also reported that the crystal structure of $La(HIBA)_2\cdot Cl\cdot 2H_2O$ formed a one-dimensional polymeric chain with HIBA ligands bridging via

dx.doi.org/10.1021/ic301775d | *Inorg. Chem.* 2012, 51, 13254–13263

the carboxylate group. Using the reported atom coordinates and thermal parameters from their crystal structure refinement, we find that the unusually brief interpretation of the structural data by Lin et al. is incorrect.[27] The bond lengths and coordination geometry of the HIBA ligand to the La(III) center are nearly identical to that reported here for **1**. While $La(HIBA)_2 \cdot Cl \cdot 2H_2O$ was originally reported as a one-dimensional polymeric chain structure, we believe the data is actually consistent with a two-dimensional sheet similar to the structure reported here for **1**.

Spectroscopic characterization of solid state and solution compounds reveals a similar coordination environment around the Ln atoms. The absence of NMR shifts for the free ligand in solution is consistent with UV−vis solution absorbance and Raman data suggesting a thermodynamically stable Ln(III)−HIBA solution complex. Similarly, ^{13}C NMR studies of the lightest lanthanide (La) and the heaviest lanthanide (Lu) system with HIBA indicate formation of a single solution complex. Both NMR and vibrational spectroscopic data clearly identify that both hydroxyl and carboxyl groups of the HIBA ligand participate in bonding the Ln atoms. The strong correlation between the solid state diffuse reflectance and the solution species absorbance spectra strengthens the suggestion that the coordination of the Ln atom is very similar in solution and the solid state. This research furthers our fundamental scientific understanding of the structure and bonding of lanthanide complexes with HIBA under conditions most relevant to physiological processes and recycling of used nuclear fuel.

■ ASSOCIATED CONTENT

Supporting Information

Crystallographic and spectroscopic data for the additional lanthanide complexes as described in the text. This material is available free of charge via the Internet at http://pubs.acs.org.

■ AUTHOR INFORMATION

Corresponding Author

*E-mail: georgeg@lanl.gov or runde@lanl.gov.

Notes

The authors declare no competing financial interest.

■ ACKNOWLEDGMENTS

The authors gratefully acknowledge the Los Alamos Laboratory Directed Research and Development Program and the G. T. Seaborg Institute for Transactinium Science at Los Alamos National Laboratory for financial support during this project.

■ REFERENCES

(1) Datta, R. Hydroxycarboxylic Acids. *Kirk-Othmer Encyclopedia of Chemical Technology*; John Wiley & Sons, Inc.: New York, 2000.

(2) Pettersen, J.; Landaas, S.; Eldjarn, L. *Clin. Chim. Acta* **1973**, *48*, 213.

(3) Srere, P. A. *Curr. Top. Cell. Regul.* **1972**, *5*, 229.

(4) Gall1, W. E.; Beebe1, K.; Lawton1, K. A.; Adam1, K.; Mitchell1, M. W.; Nakhle1, P. J.; Ryals1, J. A.; Milburn1, M. V.; Nannipieri, M.; Camastra, S.; Natali, A.; Ferrannini, E. *Plos One* **2010**, *5*, e10883.

(5) Hänninen, K.; Niemelä, K. *Acta Chem. Scand.* **1992**, *46*, 459.

(6) Bourbonniere, R. A.; Meyers, P. A. *Org. Geochem.* **1983**, *5*, 131.

(7) Crouch, E. A. C. *Atomic data and Nuclear Data Tables*; Academic Press: New York, 1977; p 502.

(8) Nash, K. L.; Choppin, G. R. *Sep. Sci. Technol.* **1997**, *32*, 255.

(9) (a) Choppin, G. R.; Silva, R. J. *J. Inorg. Nucl. Chem.* **1956**, *3*, 153. (b) Smith, H. L.; Hoffman, D. C. *J. Inorg. Nucl. Chem.* **1956**, *3*, 243.

(10) Nash, K.; Jensen, M. In *Handb. Phys. Chem. Rare Earths*; Gschneidner, K. A., Eyring, L., Eds.; Elsevier: New York, 2000; Vol. *28*, p 311.

(11) Baker, J. D.; Gehrke, R. J.; Greenwood, R. C.; Meikrantz, D. H. *Radiochim. Acta* **1981**, *28*, 51.

(12) Perdue, H. D.; Conover, A.; Sawley, N.; Anderson, R. *Anal. Chem.* **1968**, *40*, 1773.

(13) Kawabata, K.; Kishi, Y.; Kawaguchi, O.; Watanabe, Y.; Inoue, Y. *Anal. Chem.* **1991**, *63*, 2137.

(14) Schädel, M.; Brüchle, W.; Schimpf, E. *Radiochim. Acta* **1992**, *57*, 85.

(15) Malmbeck, R.; Apostolidis, C.; Carlos, R.; Glatz, J.-P.; Molinet, R.; Morgenstern, A.; Nicholl, A.; Pagliosa, G. *Radiochim. Acta* **2001**, *89*, 543.

(16) Römer1, K.; Schädel2, M.; Sätmark1, B.; N. Trautmann Janos, P. *Electrophoresis* **2003**, *24*, 1982.

(17) Datta, A.; Sivaraman, N.; Srinivasan, T. G.; Rao, P. R. V. *Radiochim. Acta* **2010**, *98*, 277.

(18) Holm, L. W.; Choppin, G. R.; Moy, D. J. *Inorg. Nucl. Chem.* **1961**, *19*, 251.

(19) Stagg, W. R.; Powell, J. E. *Inorg. Chem.* **1964**, *3*, 242.

(20) Deelstra, H.; Verbeek, F. *Anal. Chim. Acta* **1964**, *31*, 251.

(21) Smatanová, I.; Marek, J.; Švančárek, P.; Schwendt, P. *Acta Crystallogr.* **1998**, *C54*, 1249.

(22) Tacke, R.; Heermann, J.; Pfrommer, B. *Inorg. Chem.* **1998**, *37*, 2070.

(23) (a) Carballo, R.; Castiñeiras, A.; Covelo, B.; Vázquez-López, E. M. *Polyhedron* **2001**, *20*, 899. (b) Carballo, R.; Castiñeiras, A.; Balboa, S.; Covelo, B.; Niclós, J. *Polyhedron* **2002**, *21*, 2811. (c) Carballo, R.; Covelo, B.; Fernández-Hermida, N.; García-Martínez, E.; Lago, A. B.; Vázquez-López, E. M. *Cryst. Growth Des.* **2008**, *8*, 995.

(24) (a) Carballo, R.; Covelo, B.; Vázquez-López, E. M. *Z. Anorg. Allg. Chem.* **2002**, *628*, 468. (b) Carballo, R.; Covelo, B.; Vázquez-López, E. M.; García-Martínez, E.; Castiñeiras, A. *Z. Anorg. Allg. Chem.* **2003**, *629*, 584. (c) Covelo, B.; Carballo, R.; Vázquez-López, E. M.; García-Martínez, E.; Lago, A. B. *Anal. Sci.* **2006**, *22*, x123.

(25) (a) Carballo, R.; Covelo, B.; García-Martínez, E.; Vázquez-López, E. M.; Castiñeiras, A.; Niclós, J. *Polyhedron* **2003**, *22*, 1051. (b) Carballo, R.; Castiñeiras, A.; Covelo, B.; García-Martínez, E.; Niclós, J.; Vázquez-López, E. M. *Polyhedron* **2004**, *23*, 1505.

(26) Carballo, R.; Covelo, B.; Vázquez-López, E. M.; García-Martínez, E.; Castiñeiras, A.; Niclós, J. *Z. Anorg. Allg. Chem.* **2005**, *631*, 785.

(27) Lin, F.; Ni, Z.; Xu, C. *Wuji Huaxue Xuebao* **1994**, *10*, 266.

(28) Runde, W. H.; Neu, M. P.; Van Pelt, C.; Scott, B. L. *Inorg. Chem.* **2000**, *39*, 1050.

(29) Runde, W. H.; Efurd, D.; Neu, M. P.; Reilly, S. D.; VanPelt, C. E.; Conradson, S. D. *AIP Conf. Proc.* **2000**, *532*, 272.

(30) Bean, A. C.; Xu, Y.; Danis, J. A.; Albrecht-Schmitt, T. E.; Scott, B. L.; Runde, W. H. *Inorg. Chem.* **2002**, *41*, 6775.

(31) Bean, A. C.; Garcia, E.; Scott, B. L.; Runde, W. H. *Inorg. Chem.* **2004**, *43*, 6145.

(32) Peper, S. M.; Brodnax, L. F.; Field, S. E.; Zehnder, R. A.; Valdez, S. N.; Runde, W. H. *Ind. Eng. Chem. Res.* **2004**, *43*, 8188.

(33) Bean, A. C.; Abney, K.; Scott, B. L.; Runde, W. H. *Inorg. Chem.* **2005**, *44*, 5209.

(34) Goff, G. S.; Brodnax, L. F.; Cisneros, M. R.; Peper, S. M.; Field, S. E.; Scott, B. L.; Runde, W. H. *Inorg. Chem.* **2008**, *47*, 1984.

(35) Runde, W. H.; Brodnax, L. F.; Goff, G. S.; Bean, A. C.; Scott, B. L. *Inorg. Chem.* **2009**, *48*, 5967.

(36) Zehnder, R. A.; Clark, D. L.; Scott, B. L.; Donohoe, R. J.; Palmer, P. D.; Runde, W. H.; Hobart, D. E. *Inorg. Chem.* **2010**, *49*, 4781.

(37) Goff, G. S.; Cisneros, M. R.; Kluk, C.; Williamson, K.; Scott, B.; Reilly, S.; Runde, W. H. *Inorg. Chem.* **2010**, *49*, 6558.

(38) Runde, W. H.; Mincher, B. J. *Chem. Rev.* **2011**, *111*, 5723.

(39) *APEX II*; Bruker AXS, Inc.: Madison, WI, 2004.

(40) *SAINT+*; Bruker AXS, Inc.: Madison, WI, 2003.

(41) Sheldrick, G. *SADABS*; University of Gottingen: Gottingen, Germany, 2001.
(42) *SHELXTL*; Bruker AXS, Inc.: Madison, WI, 1997.
(43) Gaykema, W. P. J.; Kanters, J. A.; Roelofsen, G. *Cryst. Struct. Commun.* **1978**, *7*, 463.
(44) Shannon, R. D. *Acta Crystallogr.* **1976**, *A32*, 751.
(45) Jarmelo, S.; Fausto, R. *Phys. Chem. Chem. Phys.* **2002**, *4*, 1555.
(46) Zolin, V. F. *J. Alloys Compd.* **2004**, *380*, 101.
(47) Tyutyunnik, A. P.; Zubkov, V. G.; Krasil'nikov, V. N.; Berger, I. F.; Perelyaeva, L. A.; Baklanova, I. V.; Skripkin, M. Yu.; Svensson, G. *J. Struct. Chem.* **2011**, *52*, 350.
(48) Abbasi, A.; Risberg, E. D.; Eriksson, L.; Mink, J.; Persson, I.; Sandström, M.; Sidorov, Y. V.; Skripkin, M. Y.; Ullström, A. *Inorg. Chem.* **2007**, *46*, 7731.
(49) (a) Carnall, W. T. The Absorption and Fluoresence Spectra of Rare Earth Ions in Solution. In *Handbook on the Chemistry and Physics of the Rare Earths*; Gschneider, K. A., Jr., Eyring, L., Eds.; Chapter 24; North-Holland Publishing Company, 1979; pp 171−208. (b) Carnall, W. T.; Fields, P. R.; Rajnak, J. *J. Chem. Phys.* **1968**, *48*, 4424.
(50) Kyômen, T.; Sakamoto, R.; Sakamoto, N.; Kunugi, S.; Itoh, M. *Chem. Mater.* **2005**, *17*, 3200.
(51) Lazaridou, V.; Perlepes, S. P.; Tsangaris, J. M.; Zafiropoulos, Th. F. *J. Less-Common. Met.* **1990**, *158*, 1.